Report

Cell Reports

# The Mitochondrial Calcium Uniporter Selectively Matches Metabolic Output to Acute Contractile Stress in the Heart

## Graphical Abstract

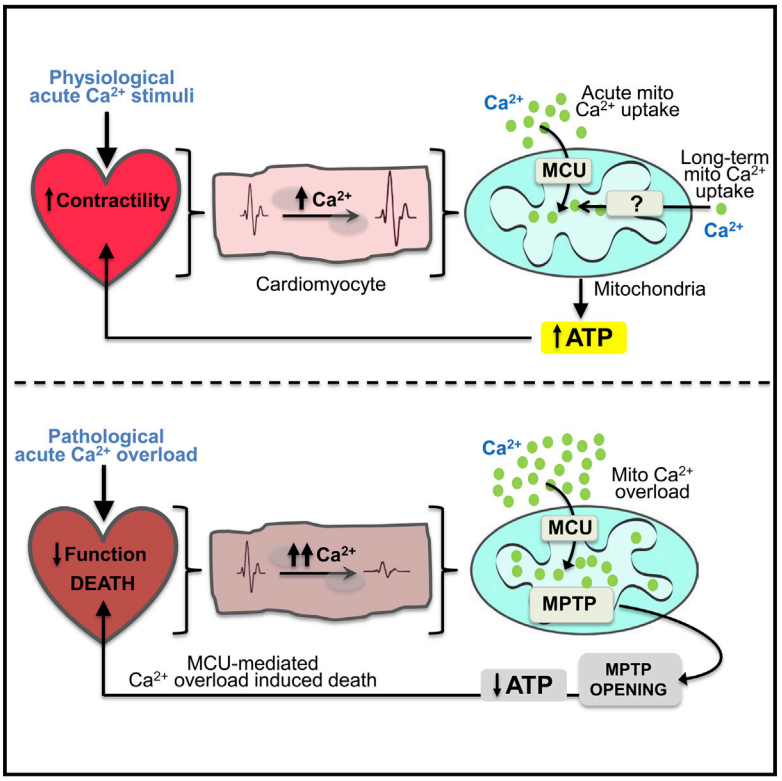


## Highlights

- Adult mice lacking MCU in the heart show no pathology or mitochondrial defects
- MCU selectively mediates acute mitochondria $Ca^{2+}$ loading to augment ATP synthesis
- In cardiac ischemic injury, MCU mediates mitochondrial $Ca^{2+}$ overload and cell death

## Authors

Jennifer Q. Kwong, Xiyuan Lu, Robert N. Correll, ..., Jianyi Zhang, Donald M. Bers, Jeffery D. Molkentin

## Correspondence

jeff.molkentin@cchmc.org

## In Brief

The mitochondrial $Ca^{2+}$ uniporter (MCU) is a critical mediator of mitochondrial $Ca^{2+}$ import, but its physiologic and pathologic roles remain unclear. Kwong et al. report MCU's essential role in acute mitochondrial $Ca^{2+}$ uptake in the heart, where it augments momentary $Ca^{2+}$-dependent mitochondrial metabolic output in response to elevated contractile demand.

Kwong et al., 2015, Cell Reports *12*, 15–22
July 7, 2015 
http://dx.doi.org/10.1016/j.celrep.2015.06.002

Cell Reports
Report



# The Mitochondrial Calcium Uniporter Selectively Matches Metabolic Output to Acute Contractile Stress in the Heart

Jennifer Q. Kwong,[1,5] Xiyuan Lu,[2,5] Robert N. Correll,[1] Jennifer A. Schwanekamp,[1] Ronald J. Vagnozzi,[1] Michelle A. Sargent,[1] Allen J. York,[1] Jianyi Zhang,[3] Donald M. Bers,[2] and Jeffery D. Molkentin[1,4,*]
[1]Department of Pediatrics, Cincinnati Children's Hospital Medical Center, University of Cincinnati, Cincinnati, OH 45229, USA
[2]Department of Pharmacology, University of California-Davis, Davis, CA 95616, USA
[3]Department of Medicine, Leilihei Heart Institute, University of Minnesota, Minneapolis, MN 55455, USA
[4]Howard Hughes Medical Institute, Cincinnati Children's Hospital Medical Center, Cincinnati, OH 45229, USA
[5]Co-first author
*Correspondence: jeff.molkentin@cchmc.org
http://dx.doi.org/10.1016/j.celrep.2015.06.002


## SUMMARY

**In the heart, augmented $Ca^{2+}$ fluxing drives contractility and ATP generation through mitochondrial $Ca^{2+}$ loading. Pathologic mitochondrial $Ca^{2+}$ overload with ischemic injury triggers mitochondrial permeability transition pore (MPTP) opening and cardiomyocyte death. Mitochondrial $Ca^{2+}$ uptake is primarily mediated by the mitochondrial $Ca^{2+}$ uniporter (MCU). Here, we generated mice with adult and cardiomyocyte-specific deletion of *Mcu*, which produced mitochondria refractory to acute $Ca^{2+}$ uptake, with impaired ATP production, and inhibited MPTP opening upon acute $Ca^{2+}$ challenge. Mice lacking *Mcu* in the adult heart were also protected from acute ischemia-reperfusion injury. However, resting/basal mitochondrial $Ca^{2+}$ levels were normal in hearts of *Mcu*-deleted mice, and mitochondria lacking MCU eventually loaded with $Ca^{2+}$ after stress stimulation. Indeed, *Mcu*-deleted mice were unable to immediately sprint on a treadmill unless warmed up for 30 min. Hence, MCU is a dedicated regulator of short-term mitochondrial $Ca^{2+}$ loading underlying a "fight-or-flight" response that acutely matches cardiac workload with ATP production.**

## INTRODUCTION

Under physiological conditions, mitochondrial $Ca^{2+}$ loading serves as a signal to enhance mitochondrial energetic output, either by directly binding and activating key dehydrogenases of the tricarboxylic acid cycle or by activation of the ATP synthase, thereby linking momentary cardiac contractile $Ca^{2+}$ cycling with metabolic output (Glancy and Balaban, 2012). However, prolonged elevations of intracellular $Ca^{2+}$ can trigger mitochondrial permeability transition pore (MPTP) opening, mitochondrial dysfunction, and cardiomyocyte death (Kwong and Molkentin, 2015).

A major pathway for mitochondrial $Ca^{2+}$ entry is through the mitochondrial $Ca^{2+}$ uniporter (MCU) complex, a selective $Ca^{2+}$ channel that facilitates the voltage-dependent transport of $Ca^{2+}$ across the mitochondrial inner membrane (Kamer et al., 2014). The core complex is comprised of the *Mcu* gene product itself that forms the pore and the regulatory subunits MICU1, MICU2, EMRE, and MCUb (Kamer et al., 2014). Specific inhibition of MCU with pharmacological agents such as ruthenium red and Ru360 (Matlib et al., 1998; Zazueta et al., 1999) as well as genetic ablation of MCU complex components blocks acute mitochondrial $Ca^{2+}$ influx (Baughman et al., 2011; De Stefani et al., 2011; Pan et al., 2013; Sancak et al., 2013). MCU inhibition via drugs or RNAi also abrogates cell death in numerous in vitro models, presumably due to less $Ca^{2+}$ influx and reduced MPTP opening (Dessi et al., 1995; Groskreutz et al., 1992; Qiu et al., 2013).

Recently, viable mice were generated with global deletion of the *Mcu* gene (Pan et al., 2013). Although mitochondria isolated from these animals had impaired acute $Ca^{2+}$ uptake, cardiac structure and function were unaffected. Moreover, whereas $Ca^{2+}$-induced MPTP opening was abrogated in purified mitochondria lacking *Mcu* (Pan et al., 2013), cardiac ischemic injury was not reduced as would be predicted from past results with Ru360 or ruthenium red (García-Rivas et al., 2006; Zhang et al., 2006). More recently, Wu and colleagues used a cardiac-specific transgenic approach to overexpress a dominant-negative MCU protein in the heart and found that MCU function was required for cardiac pacemaker cell activity to increase heart rate following catecholamine stimulation (Wu et al., 2015).

## RESULTS

### Deletion of MCU in the Heart Blocks Acute Mitochondrial $Ca^{2+}$ Uptake

To examine the immediate functional effects of the MCU in the heart, the *Mcu* locus was targeted with loxP sites (fl) flanking exons 5 and 6 to generate a conditional loss-of-function allele ($Mcu^{fl/fl}$; Figure 1A). $Mcu^{fl/fl}$ mice were then crossed with mice expressing a tamoxifen-inducible Cre recombinase (MerCreMer [MCM]) driven by the cardiomyocyte-specific α-myosin heavy

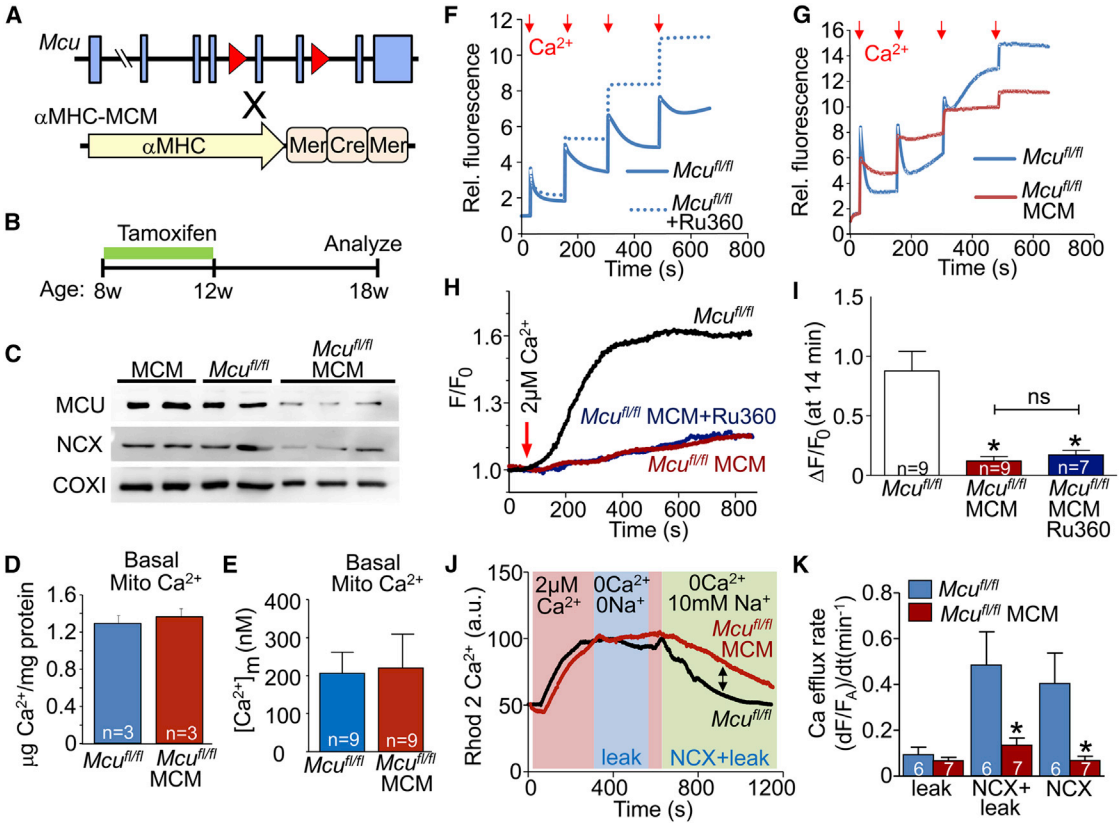


**Figure 1. Cardiomyocyte-Specific Deletion of *Mcu* Impairs Mitochondrial $Ca^{2+}$ Uptake**

(A) Targeting strategy for the *Mcu* locus to generate the $Mcu^{fl/fl}$ mice where exons 5 and 6 were flanked with LoxP sites (triangles). $Mcu^{fl/fl}$ mice were crossed to α-MHC MerCreMer (MCM) mice to generate the $Mcu^{fl/fl\text{-}MCM}$ animals.

(B) Tamoxifen dosing to induce MCM activity was given to 8-week-old animals for 4 weeks, followed by examination at 18 weeks of age.

(C) Western blots of MCU and mNCX expression in cardiac mitochondria. The COXI subunit of mitochondrial complex IV was used as a protein-loading control.

(D) Quantification of $Ca^{2+}$ content from isolated cardiac mitochondria from the indicated genotypes of mice.

(E) Quantification of free $[Ca]_m$ content in permeabilized myocytes from the indicated genotypes of mice.

(F) The effect of Ru360 (1 μM) on mitochondrial $Ca^{2+}$ uptake as measured by calcium-green 5N fluorescence in the solution. Mitochondria were challenged with 100 μM $CaCl_2$ additions (arrows).

(G) Mitochondrial $Ca^{2+}$ uptake in mitochondria from hearts of $Mcu^{fl/fl}$ versus $Mcu^{fll/fl\text{-}MCM}$ mice. Mitochondria were challenged with 200 μM $CaCl_2$ additions (arrows).

(H) Measurement of mitochondrial $Ca^{2+}$ uptake in permeabilized myocytes as assessed by Rhod-2 fluorescence in the indicated groups of mice, with or without Ru360.

(I) Quantification of Rhod-2 signal 14 min after $Ca^{2+}$ addition as shown in (H). *$p < 0.05$ versus $Mcu^{fl/fl}$. All values reported as mean ± SEM.

(J) Measurement of mitochondrial $Ca^{2+}$ efflux as mediated by mNCX and leak, assessed by Rhod-2 fluorescence in adult cardiomyocytes.

(K) Quantification of rates of mNCX $Ca^{2+}$ efflux as shown in (J). All values reported as mean ± SEM. *$p < 0.05$ versus $Mcu^{fl/fl}$.

See also Figure S1.

chain promoter (Figure 1A). *Mcu* deletion was induced in 8-week-old $Mcu^{fl/fl\text{-}MCM}$ adult mice by administration of tamoxifen food for 4 weeks followed by an additional 6-week period to allow for MCU protein turnover (Figure 1B). Following this dosing regimen, western blot analyses showed that MCU protein expression was reduced by >80% in the hearts of 18-week-old $Mcu^{fl/fl\text{-}MCM}$ animals when compared with $Mcu^{fl/fl}$ and MCM age-matched controls (Figure 1C).

Direct measurement of mitochondrial $Ca^{2+}$ levels with two different assays showed no difference in baseline mitochondrial $Ca^{2+}$ from control versus $Mcu^{fl/fl\text{-}MCM}$ hearts (Figures 1D and 1E). However, acute cardiac mitochondrial $Ca^{2+}$ uptake, as assessed with the $Ca^{2+}$-sensitive dye calcium green-5N, was dramatically inhibited (Figures 1F and 1G). $Mcu^{fl/fl}$ control cardiac mitochondria displayed typical mitochondrial $Ca^{2+}$ uptake with repeated $Ca^{2+}$ additions, reflected as the rapid decrease in fluorescence signal in the test solution after each $Ca^{2+}$ pulse, which was inhibited with Ru360 (Figure 1F). Similar to the Ru360 treatment, cardiac mitochondria from $Mcu^{fl/f\text{-}MCM}$ mice also displayed inhibited mitochondrial $Ca^{2+}$ uptake (Figure 1G).

Mitochondrial $Ca^{2+}$ handling was also measured in permeabilized adult cardiac myocytes isolated from 18-week-old $Mcu^{fl/fl}$ and $Mcu^{fl/fl\text{-}MCM}$ mice loaded with Rhod-2, a $Ca^{2+}$-sensitive dye that accumulates in mitochondria. In this assay, permeabilized $Mcu^{fl/fl}$ control myocytes challenged with 2 μM $Ca^{2+}$ displayed a robust increase in mitochondrial $Ca^{2+}$ levels that was

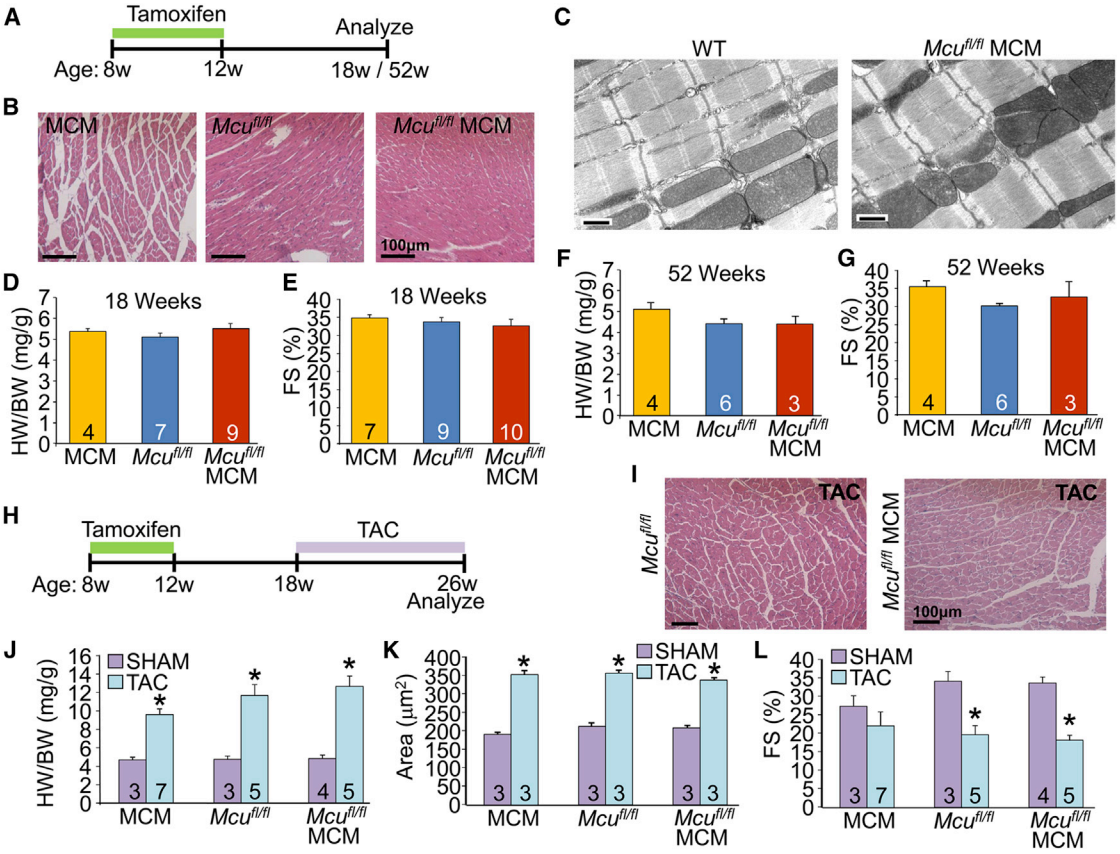


**Figure 2. Loss of MCU from the Adult Heart Does Not Lead to Pathology at Baseline or with Pathologic Stress Stimulation**

(A) Time course for the analyses of cardiac function in response to aging following *Mcu* deletion.

(B) Transverse H&E heart sections at 200× magnification.

(C) Representative electron micrographs from heart sections. The scale bar represents 500 nm.

(D) Heart-weight normalized to body-weight ratios (HW/BW) at 18 weeks of age.

(E) Echocardiographic measurement of fractional shortening (FS%) at 18 weeks of age.

(F) Heart-weight normalized to HW/BW at 52 weeks of age.

(G) Echocardiographic measurement of FS% at 52 weeks of age.

(H) Time course for generation of mice and analyses of cardiac function following TAC surgery.

(I) H&E-stained transverse heart sections 8 weeks after TAC surgery at 200× magnification.

(J–L) HW/BW (J), cardiomyocyte cross-sectional area (K), and FS% (L) in the indicated groups of mice 8 weeks following TAC.

All values reported as mean ± SEM. *$p < 0.05$ versus $Mcu^{fl/fl}$ sham.

severely blunted in *Mcu*-deficient cardiomyocytes (Figures 1H and 1I). Importantly, Ru360 treatment of $Mcu^{fl/fl\text{-}MCM}$ cardiomyocytes did not confer additional inhibition of mitochondrial $Ca^{2+}$ uptake (Figures 1H and 1I).

To understand how basal mitochondrial $Ca^{2+}$ content can remain unchanged in the face of impaired MCU activity, we examined the mitochondrial $Na^+/Ca^{2+}$ exchanger (mNCX), which is the major pathway of mitochondrial $Ca^{2+}$ efflux. Adult cardiac myocytes were isolated from $Mcu^{fl/fl\text{-}MCM}$ and $Mcu^{fl/fl}$ control animals, and mitochondria were loaded with Rhod2 and $Ca^{2+}$ by ionophore permeabilization in conjunction with Ru360 treatment and exposure to buffer containing 2 μM $Ca^{2+}$. To assess the rate of basal mitochondrial $Ca^{2+}$ efflux and leak, myocytes were exposed to buffer devoid of both $Ca^{2+}$ and $Na^+$ and then switched to a buffer containing 10 mM $Na^+$ (Figures 1J and 1K). The data show that, whereas leak rates in solution lacking $Na^+$ and $Ca^{2+}$ were similar, the $Na^+$-induced $Ca^{2+}$ efflux rate (mediated via mNCX) was much lower in *Mcu*-deleted myocytes (Figures 1J and 1K). Interestingly, deletion of *Mcu* resulted in reduced mNCX protein expression, which likely serves as the basis for the observed compensatory decrease in mNCX activity in the absence of MCU (Figure 1C).

## MCU Does Not Regulate Cardiac Adaptation to Long-Term Stress

Despite the defect in acute mitochondrial $Ca^{2+}$ uptake observed in the hearts of 18-week-old $Mcu^{fl/fl\text{-}MCM}$ animals, we observed no pathologic effects such as changes in cellular morphology, myofilament or mitochondrial ultrastructure, hypertrophic growth, or cardiac ventricular performance at 18 or even 52 weeks of aging (Figures 2A–2G). Furthermore, total cardiomyocyte $Ca^{2+}$-transient kinetics and amplitude were unaltered, and

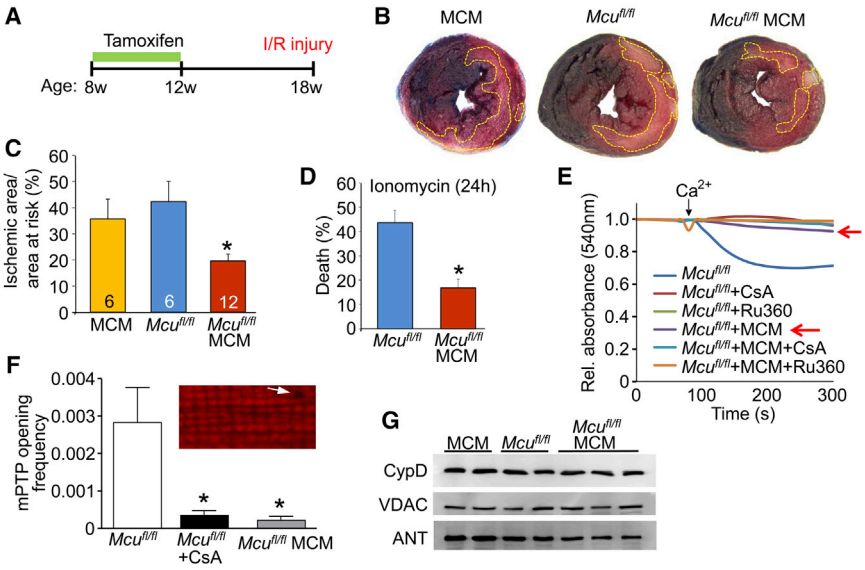


**Figure 3. MCU Is Required for Acute Mitochondrial $Ca^{2+}$ Stress Signaling**

(A) Time course for the cardiac ischemia-reperfusion experiment.

(B) Representative images of transverse heart sections stained with 2,3,5-triphenyltetrazolium chloride following ischemia-reperfusion injury from the indicated groups. Ischemic area is outlined in yellow.

(C) Quantification of the ischemic area versus area at risk. *$p < 0.05$ versus all other groups. All values presented as mean ± SEM.

(D) Cardiomyocyte viability in response to ionomycin treatment (625 nM; 24 hr). *$p < 0.05$ versus control. All values presented as mean ± SEM.

(E) Mitochondrial swelling in response to $Ca^{2+}$ challenge (200 μM $CaCl_2$). Controls were 5 μM cyclosporine A (CsA) and 2 μM Ru360. The red arrows show the critical experimental group where swelling is inhibited with *Mcu* deletion alone.

(F) Quantification of MPTP opening frequency in permeabilized cardiomyocytes. MPTP opening is measured by loss of mitochondrial membrane potential (TMRM signal; inset). Myocytes were challenged with 100 nM free $Ca^{2+}$, and 1 μM CsA was used as a control. *$p < 0.005$ versus control. All values presented as mean ± SEM.

(G) Western blots of CypD, VDAC, and ANT protein expression in purified cardiac mitochondria from the indicated genotypes of mice.

sarcoplasmic reticulum $Ca^{2+}$ load was unchanged in $Mcu^{fl/fl\text{-}MCM}$ myocytes as compared to $Mcu^{fl/fl}$ controls (Figure S1). Taken together, these results demonstrate that MCU-mediated mitochondrial $Ca^{2+}$ import neither contributes to overall cardiac $Ca^{2+}$ cycling in the heart nor is it required to support normal cardiac function and adaptation with aging.

Mouse models with subtle perturbations in baseline cardiac metabolic function or metabolic reserve often display increased pathology under stress stimulation, such as with transverse aortic constriction (TAC) (Abel and Doenst, 2011; Arany et al., 2006; Smeets et al., 2008; Wu et al., 2012). Hence, we subjected $Mcu^{fl/fl\text{-}MCM}$, $Mcu^{fl/fl}$, and MCM control mice to 8 weeks of cardiac pressure overload with TAC surgery (Figure 2H). All three groups of mice showed identical pathologic profiles in response to TAC (Figures 2I–2L). These results suggest that cardiac adaptation to chronic pressure overload is not dependent on MCU-mediated mitochondrial $Ca^{2+}$ import.

## MCU Mediates Acute Mitochondrial $Ca^{2+}$ Overload In Vivo

We next sought to determine whether MCU played a more-selective role in regulating acute $Ca^{2+}$ responses in the heart, such as after immediate ischemia-reperfusion injury. Here, 18-week-old $Mcu^{fl/fl\text{-}MCM}$ mice and age-matched $Mcu^{fl/fl}$ and MCM control animals were subjected to 1 hr of cardiac ischemia followed by 24 hr of reperfusion (Figure 3A). Consistent with past data using Ru360 or ruthenium red, mice with adult and cardiac-specific deletion of *Mcu* displayed an ~50% reduction in infarct size compared to $Mcu^{fl/fl}$ and MCM controls (Figures 3B and 3C). Correspondingly, *Mcu* deletion in cultured adult cardiomyocytes also conferred protection against acute ionomycin-induced $Ca^{2+}$ overload cell death (Figure 3D). Mechanistically, acute $Ca^{2+}$-induced MPTP opening, as measured in isolated cardiac mitochondria, was greatly desensitized in $Mcu^{fl/fl\text{-}MCM}$ mitochondria as compared to $Mcu^{fl/fl}$ controls (Figure 3E). Analyses of MPTP opening in permeabilized adult cardiomyocytes, as reflected by loss of mitochondrial membrane potential, showed inhibition with *Mcu* deletion, which was similar to cyclosporine A (CsA) treatment of WT control myocytes (Figure 3F). Importantly, expression of MPTP components such as CypD (cyclophilin D), VDAC (voltage-dependent anion channel), and ANT (adenine nucleotide translocator) were unaltered with *Mcu* deletion (Figure 3G). These results suggest that loss of MCU in the heart inhibits acute $Ca^{2+}$-induced MPTP opening, resulting in decreased cardiomyocyte damage in response to ischemia-reperfusion injury.

## MCU Is Required for Acute Mitochondrial Metabolic-Contraction Coupling

Oxygen consumption and ATP generation were examined in isolated mitochondria in response to acute $Ca^{2+}$ loading. At baseline, $Mcu^{fl/fl\text{-}MCM}$ and $Mcu^{fl/fl}$ control mitochondria displayed similar rates of mitochondrial oxygen consumption and ATP synthesis, consistent with unchanged basal $Ca^{2+}$ levels in the absence of MCU protein (Figures 4A and 4B). Furthermore, potential alternative pathways of oxidation such as reactive oxygen species (ROS) production, NADPH oxidation, superoxide dismutase 2 (SOD2) levels, and catalase activity were also unaltered with *Mcu* deletion (Figure S2). However, whereas addition of exogenous $Ca^{2+}$ to $Mcu^{fl/fl}$ control mitochondria resulted in an approximate 2-fold increase in respiration and ATP production, this acute effect was blocked by both *Mcu* deletion and addition of Ru360 to WT control mitochondria (Figures 4A and 4B).

To further investigate the hypothesis that MCU is mostly dedicated to short-term mitochondrial $Ca^{2+}$ regulation, we had to employ an intact system that could sustain extended measurements, such as isolated adult cardiac myocytes treated with the β-adrenergic receptor agonist isoproterenol. Similar to the

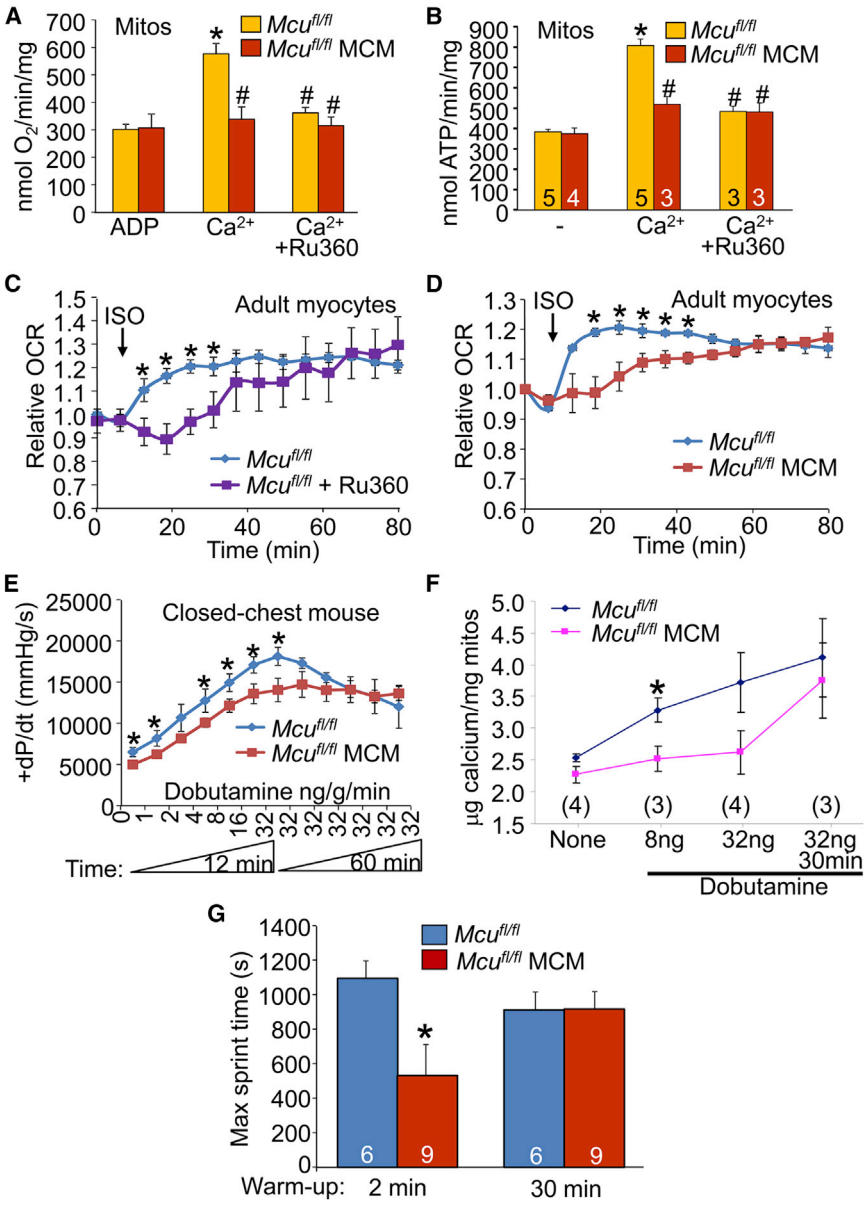


**Figure 4. Acute versus Chronic Regulation of Mitochondrial $Ca^{2+}$ and Metabolism due to MCU Activity**

(A) State 3 mitochondrial oxygen consumption in purified cardiac mitochondria from the indicated mice stimulated with 100 μM $Ca^{2+}$ with or without 2 μM Ru360. *p < 0.05 versus ADP baseline; #p < 0.05 versus $Mcu^{fl/fl}$ $Ca^{2+}$. All values presented as mean ± SEM.

(B) Mitochondrial ATP synthesis in isolated mitochondria at baseline and stimulated with 400 μM $CaCl_2$. Five micromolar Ru360 was used as a control. *p < 0.05 versus ADP baseline; #p < 0.05 versus $Mcu^{fl/fl}$ $Ca^{2+}$. All values presented as mean ± SEM.

(C) Relative oxygen consumption rates (OCR) of $Mcu^{fl/fl}$ control adult cardiomyocytes with or without Ru360 (5 μM) in response to 3.125 nM isoproterenol (ISO).

(D) OCR in $Mcu^{fl/fl\text{-}MCM}$ versus $Mcu^{fl/fl}$ adult cardiomyocytes in response to 3.125 nM isoproterenol. *p < 0.05 versus control. All values presented as mean ± SEM.

(E) Maximal rates of cardiac contraction as measured in a closed-chest mouse in response to increasing doses of dobutamine. Dobutamine was increased from 0 to 32 ng/g/min and then maintained at 32 ng/g/min for an additional hour. *p < 0.05 versus control. All values presented as mean ± SEM.

(F) Total mitochondrial $Ca^{2+}$ content measured from hearts taken at the indicated time points from indicated groups of mice following dobutamine administration of the experiment shown in (E). *p < 0.05 versus control. All values presented as mean ± SEM.

(G) Treadmill performance as quantified by maximum sprint time in the $Mcu^{fl/fl\text{-}MCM}$ versus $Mcu^{fl/fl}$ controls. Animals were subjected to two different protocols, where they were allowed either a 2-min warm-up or a 30-min warm-up before reaching maximum sprint speed. *p < 0.05 versus control. Number of mice used is shown in the bars. All values presented as mean ± SEM.

See also Figures S2 and S3.

$Ca^{2+}$-induced increase in mitochondrial respiration observed in isolated mitochondria (Figure 4A), isoproterenol treatment elicited an immediate increase in oxygen consumption in WT, but not *Mcu*-deleted, cardiomyocytes or with Ru360 pretreatment (Figures 4C and 4D). However, over the course of 80 min, the isoproterenol-stimulated oxygen consumption of the Ru360-inhibited and *Mcu*-deleted myocytes slowly caught up to the rates observed in control myocytes (Figures 4C and 4D). These results suggest that MCU is specialized for acute matching of mitochondrial energy output with cardiac metabolic demands but that long-term $Ca^{2+}$ homeostasis can be achieved through other influx pathways.

We also performed in vivo hemodynamic measurements on $Mcu^{fl/fl\text{-}MCM}$ and $Mcu^{fl/fl}$ control mice challenged with increasing concentrations of the β-adrenergic receptor agonist dobutamine. $Mcu^{fl/fl}$ control mice showed a greater short-term increase in the maximal rates of cardiac pressure developed (+dP/dt) compared to $Mcu^{fl/fl\text{-}MCM}$ animals (Figure 4E). However, with sustained administration of dobutamine at 32 ng/g/min, the $Mcu^{fl/fl\text{-}MCM}$ animals were eventually able to achieve similar maximal rates of ventricular pressure developed as compared to $Mcu^{fl/fl}$ controls (Figure 4E). Correspondingly, measurement of total cardiac mitochondrial $Ca^{2+}$ content in $Mcu^{fl/fl\text{-}MCM}$ and $Mcu^{fl/fl}$ mice showed that, whereas levels were not different at baseline, short-term administration of dobutamine resulted in significantly elevated $Ca^{2+}$ in only the $Mcu^{fl/fl}$ control mitochondria (Figure 4F). However, following 30 min of sustained dobutamine, the $Ca^{2+}$ levels in the $Mcu^{fl/fl\text{-}MCM}$ mitochondria were substantially higher and had caught up to those observed in $Mcu^{fl/fl}$ controls (Figure 4F).

Finally, we challenged $Mcu^{fl/fl\text{-}MCM}$ and $Mcu^{fl/fl}$ control animals with two contrasting treadmill-running regimens to probe further into the acute versus chronic physiologic mechanisms of MCU function (Figure S3). In the first protocol, animals were subjected to high-intensity sprinting for 20 min at a speed of 20 m/min but with only a 2-min warm-up period. In the second protocol, animals were allowed a 30-min warm-up period prior to the 20-min sprinting phase at 20 m/min (Figure S3). Under the short warm-up/high-intensity sprinting regimen, $Mcu^{fl/fl\text{-}MCM}$ animals displayed significantly reduced running capacity as compared to $Mcu^{fl/fl}$ controls, but this difference was lost if the mice were allowed a long warm-up period (Figure 4G).

## DISCUSSION

In this study, we demonstrate that the role of MCU in the heart is to acutely match augmented cardiac work with mitochondrial energy output through mitochondrial $Ca^{2+}$ loading. Indeed, loss of MCU from the heart resulted in a selective inability to acutely respond to β-adrenergic receptor stimulation or maximal forced exercise by augmenting cardiac metabolic capacity as cardiomyocyte work is enhanced. However, MCU-deficient cardiomyocytes or deficient mice eventually catch up to controls in their contractile or metabolic performance, as does total $Ca^{2+}$ load in the mitochondria.

The proposed model that MCU controls acute mitochondrial $Ca^{2+}$ entry is also supported by results observed under pathologic conditions. After cardiac ischemia-reperfusion injury, *Mcu* deletion in the adult heart was protective, a finding that recapitulates the cardioprotection observed with acute Ru360-mediated MCU inhibition in adult animals (García-Rivas et al., 2006; Zhang et al., 2006). This result is also consistent with an acute regulatory role for MCU in loading mitochondria with excessive $Ca^{2+}$ leading to catastrophic MPTP opening and myocyte necrosis. Whereas cardioprotection was not observed with the constitutive *Mcu* deletion described earlier (Pan et al., 2013), it should be noted that our targeting approach allowed us to examine uncompensated effects of MCU deletion in the adult heart, thereby circumventing the potential confounding metabolic alterations accompanying long-term and total body MCU loss. Indeed, total somatic *Mcu*-deleted mice displayed growth defects, lactic acidosis, and constitutive phosphorylation of the E1α subunit of the pyruvate dehydrogenase complex (Pan et al., 2013). Such effects were not observed in our adult and cardiac-specific *Mcu*-deleted mice (Figure S2).

Our proposed model also suggests that baseline mitochondrial $Ca^{2+}$ levels could be regulated by one or more additional influx pathways, either with or independent of MCU. For example, Graier and colleagues showed that as many as five different $Ca^{2+}$ influx currents can be identified in mitoplasts (Jean-Quartier et al., 2012), and a new current was identified in mitoplasts from cells with knockdown of MCU (Bondarenko et al., 2013). In addition, Letm1 is an $H^+/Ca^{2+}$ antiporter that can mediate energy-dependent $Ca^{2+}$ uptake into mitochondria at low cytosolic $Ca^{2+}$ concentration (Jiang et al., 2013). Finally, both the ryanodine receptor 1 (RyR1) and transient receptor potential canonical 3 (TRPC3) have been shown to mediate $Ca^{2+}$ influx into mitochondria independent of the MCU (Beutner et al., 2001; Feng et al., 2013). One known compensatory alteration that we did observe was a significant downregulation in mNCX protein expression and activity, which should partially offset the reduction in acute $Ca^{2+}$ influx, hence better maintaining overall calcium homeostasis. In summary, we conclude that MCU is the acute fight-or-flight mediator of $Ca^{2+}$ influx that facilitates immediate increases in mitochondrial metabolism and ATP production associated with augmented cardiac contractile performance.

## EXPERIMENTAL PROCEDURES

### Animals

The *Mcu* gene-targeting strategy and generation of the *Mcu* chimeric mice was through the Howard Hughes Medical Institute Gene Targeting Core (Figure S4). These same mice were also provided to Dr. John Elrod for their use in a co-submitted manuscript published in this same issue (Luongo et al., 2015). Homozygous $Mcu^{fl/fl}$ mice were bred to transgenic mice expressing the tamoxifen-inducible Cre recombinase under the control of the α-MHC promoter (Sohal et al., 2001). All animal experiments were approved and performed in accordance by Children's Hospital Medical Center's Institutional Animal Care and Use Committee.

### Cardiac Functional Analyses, Surgical Procedures, and Treadmill Running

Echocardiography was performed using a Hewlett Packard SONOS 5500 imaging system as previously described (Nakayama et al., 2009). The TAC model of cardiac pressure overload was performed as described previously (Kaiser et al., 2004). Ischemia-reperfusion injury was performed as previously described (Wilkins et al., 2004). Adult cardiac myocytes were isolated as previously described (Goonasekera et al., 2012). The enforced sprinting protocols were performed using an Omni-Pacer LC4/M treadmill (Columbus Instruments International) and diagrammed in Figure S3.

### Respiration in Adult Cardiomyocytes

Respiration in adult cardiomyocytes was measured using a Seahorse XF24 Flux Analyzer (Seahorse Biosciences) as described in Readnower et al. (2012).

### Mitochondrial Isolation and Analyses

Cardiac mitochondria were isolated as previously described (Kwong et al., 2014). Mitochondrial ATP synthesis rates were measured as described in Vives-Bauza et al. (2007). Mitochondrial swelling assays were conducted as previously described (Kwong et al., 2014).

### $Ca^{2+}$ Sparks and Transients Measurements

Intact ventricular myocytes were loaded with Fluo-4 AM dye (5 μM Molecular Probes), and transients and sparks were recorded as previously described (Erickson et al., 2013; van Oort et al., 2010).

### Statistics

All results are presented as mean ± SEM. Statistical significance was determined by Student's t test, and p values $< 0.05$ were considered significant.

## SUPPLEMENTAL INFORMATION

Supplemental Information includes Supplemental Experimental Procedures and four figures and can be found with this article online at http://dx.doi.org/10.1016/j.celrep.2015.06.002.

## AUTHOR CONTRIBUTIONS

J.D.M. and J.Q.K. wrote the manuscript. J.Q.K., X.L., R.N.C., R.J.V., M.A.S., J.A.S., and A.J.Y. performed experimentation. J.D.M., J.Z., and D.M.B provided experimental oversight and helped design the study.

## ACKNOWLEDGMENTS

This work was supported by grants from the NIH (J.D.M., J.Z., and D.M.B.) and the Howard Hughes Medical Institute (J.D.M.). J.Q.K. was supported by an American Heart Association Local Affiliate Grant.

Received: March 6, 2015
Revised: April 15, 2015
Accepted: May 30, 2015
Published: June 25, 2015

## REFERENCES

Abel, E.D., and Doenst, T. (2011). Mitochondrial adaptations to physiological vs. pathological cardiac hypertrophy. Cardiovasc. Res. *90*, 234–242.

Arany, Z., Novikov, M., Chin, S., Ma, Y., Rosenzweig, A., and Spiegelman, B.M. (2006). Transverse aortic constriction leads to accelerated heart failure in mice lacking PPAR-gamma coactivator 1alpha. Proc. Natl. Acad. Sci. USA *103*, 10086–10091.

Baughman, J.M., Perocchi, F., Girgis, H.S., Plovanich, M., Belcher-Timme, C.A., Sancak, Y., Bao, X.R., Strittmatter, L., Goldberger, O., Bogorad, R.L., et al. (2011). Integrative genomics identifies MCU as an essential component of the mitochondrial calcium uniporter. Nature *476*, 341–345.

Beutner, G., Sharma, V.K., Giovannucci, D.R., Yule, D.I., and Sheu, S.S. (2001). Identification of a ryanodine receptor in rat heart mitochondria. J. Biol. Chem. *276*, 21482–21488.

Bondarenko, A.I., Jean-Quartier, C., Malli, R., and Graier, W.F. (2013). Characterization of distinct single-channel properties of $Ca^{2+}$ inward currents in mitochondria. Pflugers Arch. *465*, 997–1010.

De Stefani, D., Raffaello, A., Teardo, E., Szabò, I., and Rizzuto, R. (2011). A forty-kilodalton protein of the inner membrane is the mitochondrial calcium uniporter. Nature *476*, 336–340.

Dessi, F., Ben-Ari, Y., and Charriaut-Marlangue, C. (1995). Ruthenium red protects against glutamate-induced neuronal death in cerebellar culture. Neurosci. Lett. *201*, 53–56.

Erickson, J.R., Pereira, L., Wang, L., Han, G., Ferguson, A., Dao, K., Copeland, R.J., Despa, F., Hart, G.W., Ripplinger, C.M., and Bers, D.M. (2013). Diabetic hyperglycaemia activates CaMKII and arrhythmias by O-linked glycosylation. Nature *502*, 372–376.

Feng, S., Li, H., Tai, Y., Huang, J., Su, Y., Abramowitz, J., Zhu, M.X., Birnbaumer, L., and Wang, Y. (2013). Canonical transient receptor potential 3 channels regulate mitochondrial calcium uptake. Proc. Natl. Acad. Sci. USA *110*, 11011–11016.

García-Rivas, Gde.J., Carvajal, K., Correa, F., and Zazueta, C. (2006). Ru360, a specific mitochondrial calcium uptake inhibitor, improves cardiac post-ischaemic functional recovery in rats in vivo. Br. J. Pharmacol. *149*, 829–837.

Glancy, B., and Balaban, R.S. (2012). Role of mitochondrial Ca2+ in the regulation of cellular energetics. Biochemistry *51*, 2959–2973.

Goonasekera, S.A., Hammer, K., Auger-Messier, M., Bodi, I., Chen, X., Zhang, H., Reiken, S., Elrod, J.W., Correll, R.N., York, A.J., et al. (2012). Decreased cardiac L-type $Ca^{2+}$ channel activity induces hypertrophy and heart failure in mice. J. Clin. Invest. *122*, 280–290.

Groskreutz, J.L., Bronk, S.F., and Gores, G.J. (1992). Ruthenium red delays the onset of cell death during oxidative stress of rat hepatocytes. Gastroenterology *102*, 1030–1038.

Jean-Quartier, C., Bondarenko, A.I., Alam, M.R., Trenker, M., Waldeck-Weiermair, M., Malli, R., and Graier, W.F. (2012). Studying mitochondrial Ca(2+) uptake - a revisit. Mol. Cell. Endocrinol. *353*, 114–127.

Jiang, D., Zhao, L., Clish, C.B., and Clapham, D.E. (2013). Letm1, the mitochondrial Ca2+/H+ antiporter, is essential for normal glucose metabolism and alters brain function in Wolf-Hirschhorn syndrome. Proc. Natl. Acad. Sci. USA *110*, E2249–E2254.

Kaiser, R.A., Bueno, O.F., Lips, D.J., Doevendans, P.A., Jones, F., Kimball, T.F., and Molkentin, J.D. (2004). Targeted inhibition of p38 mitogen-activated protein kinase antagonizes cardiac injury and cell death following ischemia-reperfusion in vivo. J. Biol. Chem. *279*, 15524–15530.

Kamer, K.J., Sancak, Y., and Mootha, V.K. (2014). The uniporter: from newly identified parts to function. Biochem. Biophys. Res. Commun. *449*, 370–372.

Kwong, J.Q., and Molkentin, J.D. (2015). Physiological and pathological roles of the mitochondrial permeability transition pore in the heart. Cell Metab. *21*, 206–214.

Kwong, J.Q., Davis, J., Baines, C.P., Sargent, M.A., Karch, J., Wang, X., Huang, T., and Molkentin, J.D. (2014). Genetic deletion of the mitochondrial phosphate carrier desensitizes the mitochondrial permeability transition pore and causes cardiomyopathy. Cell Death Differ. *21*, 1209–1217.

Luongo, T.S., Lambert, J.P., Yuan, A., Zhang, X., and Gross, P. (2015). The Mitochondrial Calcium Uniporter Matches Energetic Supply with Cardiac Workload during Stress and Modulates Permeability Transition. Cell Rep. *12*, Published online June 25, 2015. http://dx.doi.org/10.1016/j.celrep.2015.06.017.

Matlib, M.A., Zhou, Z., Knight, S., Ahmed, S., Choi, K.M., Krause-Bauer, J., Phillips, R., Altschuld, R., Katsube, Y., Sperelakis, N., and Bers, D.M. (1998). Oxygen-bridged dinuclear ruthenium amine complex specifically inhibits Ca2+ uptake into mitochondria in vitro and in situ in single cardiac myocytes. J. Biol. Chem. *273*, 10223–10231.

Nakayama, H., Bodi, I., Correll, R.N., Chen, X., Lorenz, J., Houser, S.R., Robbins, J., Schwartz, A., and Molkentin, J.D. (2009). alpha1G-dependent T-type Ca2+ current antagonizes cardiac hypertrophy through a NOS3-dependent mechanism in mice. J. Clin. Invest. *119*, 3787–3796.

Pan, X., Liu, J., Nguyen, T., Liu, C., Sun, J., Teng, Y., Fergusson, M.M., Rovira, I.I., Allen, M., Springer, D.A., et al. (2013). The physiological role of mitochondrial calcium revealed by mice lacking the mitochondrial calcium uniporter. Nat. Cell Biol. *15*, 1464–1472.

Qiu, J., Tan, Y.W., Hagenston, A.M., Martel, M.A., Kneisel, N., Skehel, P.A., Wyllie, D.J., Bading, H., and Hardingham, G.E. (2013). Mitochondrial calcium uniporter Mcu controls excitotoxicity and is transcriptionally repressed by neuroprotective nuclear calcium signals. Nat. Commun. *4*, 2034.

Readnower, R.D., Brainard, R.E., Hill, B.G., and Jones, S.P. (2012). Standardized bioenergetic profiling of adult mouse cardiomyocytes. Physiol. Genomics *44*, 1208–1213.

Sancak, Y., Markhard, A.L., Kitami, T., Kovács-Bogdán, E., Kamer, K.J., Udeshi, N.D., Carr, S.A., Chaudhuri, D., Clapham, D.E., Li, A.A., et al. (2013). EMRE is an essential component of the mitochondrial calcium uniporter complex. Science *342*, 1379–1382.

Smeets, P.J., Teunissen, B.E., Willemsen, P.H., van Nieuwenhoven, F.A., Brouns, A.E., Janssen, B.J., Cleutjens, J.P., Staels, B., van der Vusse, G.J., and van Bilsen, M. (2008). Cardiac hypertrophy is enhanced in PPAR alpha-/- mice in response to chronic pressure overload. Cardiovasc. Res. *78*, 79–89.

Sohal, D.S., Nghiem, M., Crackower, M.A., Witt, S.A., Kimball, T.R., Tymitz, K.M., Penninger, J.M., and Molkentin, J.D. (2001). Temporally regulated and tissue-specific gene manipulations in the adult and embryonic heart using a tamoxifen-inducible Cre protein. Circ. Res. *89*, 20–25.

van Oort, R.J., Respress, J.L., Li, N., Reynolds, C., De Almeida, A.C., Skapura, D.G., De Windt, L.J., and Wehrens, X.H. (2010). Accelerated development of pressure overload-induced cardiac hypertrophy and dysfunction in an RyR2-R176Q knockin mouse model. Hypertension *55*, 932–938.

Vives-Bauza, C., Yang, L., and Manfredi, G. (2007). Assay of mitochondrial ATP synthesis in animal cells and tissues. Methods Cell Biol. *80*, 155–171.

Wilkins, B.J., Dai, Y.S., Bueno, O.F., Parsons, S.A., Xu, J., Plank, D.M., Jones, F., Kimball, T.R., and Molkentin, J.D. (2004). Calcineurin/NFAT coupling participates in pathological, but not physiological, cardiac hypertrophy. Circ. Res. *94*, 110–118.

Wu, R., Wyatt, E., Chawla, K., Tran, M., Ghanefar, M., Laakso, M., Epting, C.L., and Ardehali, H. (2012). Hexokinase II knockdown results in exaggerated cardiac hypertrophy via increased ROS production. EMBO Mol. Med. *4*, 633–646.

Wu, Y., Rasmussen, T.P., Koval, O.M., Joiner, M.L., Hall, D.D., Chen, B., Luczak, E.D., Wang, Q., Rokita, A.G., Wehrens, X.H., et al. (2015). The mitochondrial uniporter controls fight or flight heart rate increases. Nat. Commun. *6*, 6081.

Zazueta, C., Sosa-Torres, M.E., Correa, F., and Garza-Ortiz, A. (1999). Inhibitory properties of ruthenium amine complexes on mitochondrial calcium uptake. J. Bioenerg. Biomembr. *31*, 551–557.

Zhang, S.Z., Gao, Q., Cao, C.M., Bruce, I.C., and Xia, Q. (2006). Involvement of the mitochondrial calcium uniporter in cardioprotection by ischemic preconditioning. Life Sci. *78*, 738–745.

**Cell Reports**

**Supplemental Information**

# The Mitochondrial Calcium Uniporter Selectively Matches Metabolic Output to Acute Contractile Stress in the Heart

**Jennifer Q. Kwong, Xiyuan Lu, Robert N. Correll, Jennifer A. Schwanekamp, Ronald J. Vagnozzi, Michelle A. Sargent, Allen J. York, Jianyi Zhang, Donald M. Bers, and Jeffery D. Molkentin**

## Extended Methods

### Animals

The *Mcu* gene targeting strategy and generation of the *Mcu* chimeric mice was through the Howard Hughes Medical Institute Gene Targeting Core (Figure S4). Briefly, the targeting vector was designed for the *Mcu* gene to insert loxP sites flanking exons 5 and 6 for homologous recombination in embryonic stem cells (129S6 x C57BL/6J hybrid). Correctly targeted embryonic stem cells were aggregated with 8 cell stage CD1 embryos to make chimeric mice, which were then bred with C57BL/6 mice to obtain germline transmission. $Mcu^{fl/+}$ mice were first crossed to Flp mice (B6.129S4-Gt(ROSA)26Sortm1(FLP1)Dym/RainJ; Jackson Laboratories) to delete the neomycin cassette, backcrossed to C57BL/6J mice, bred to homozygosity ($Mcu^{fl/fl}$) and then bred to transgenic mice expressing the tamoxifen inducible Cre recombinase under the control of the $\alpha$-MHC promoter (Sohal et al., 2001). Cre-mediated *Mcu* excision was induced at 8 weeks of age with tamoxifen food (Harlan, 400mg/kg for 4 weeks). For histological analyses, hearts were embedded in paraffin, and 5 $\mu$m histological sections were cut and stained with hematoxylin and eosin. Cross sectional area of greater than 200 cardiomyocytes per group was measured using NIH Image J Software. Electron microscopy was performed as previously described in (Fewell et al., 1997) using a Hitachi 7600 transmission electron microscope. All animal experiments were approved and performed in accordance by Cincinnati Children's Hospital Medical Center's Institutional Animal Care and Use Committee.

### Western blot analyses.

Proteins were solubilized in RIPA buffer containing protease and phosphatase inhibitors. Proteins were resolved on 10% acrylamide gels, transferred on to PVDF membranes and immunoblotted for: MCU (Cell Signaling), mNCX (Abcam), COXI (Abcam), SOD2 (Santa Cruz), phosphorylated PDHE1$\alpha$ Ser293 (Millipore) GADPH (Fitzgerald), VDAC (Abcam), ANT (Abcam) and CypD (Abcam). The blots were washed and incubated with the appropriate secondary antibody conjugated to alkaline phosphatase at 1:2500. Blots were then exposed using chemiluminescence detection reagent to visualize bands (GE Healthcare Biosciences, Pittsburgh, PA).

### Cardiac functional analyses and surgical procedures and treadmill running

Echocardiography was performed using a Hewlett Packard SONOS 5500 imaging system with a 15-MHz transducer as previously described (Nakayama et al., 2009). The transverse aortic

constriction model of cardiac pressure overload was performed as described previously (Kaiser et al., 2004). Briefly, mice were subjected to ligation of the transverse aortic arch between the right brachiocephalic and left common carotid arteries around a 27-gauge needle. Sham operated control animals were subjected to a surgery where the transverse aortic arch was not ligated. Ischemia-reperfusion injury was performed as previously described (Wilkins et al., 2004). Animals were subjected to left descending coronary artery (LAD) occlusion for 60 minutes and reperfusion for 24 hours. Following reperfusion, the LAD was re-occluded and Evans blue dye was injected into the left ventricle to visualize the nonischemic area. Hearts were excised, embedded in 2% agarose, sectioned and stained with 2% 2,3,5-triphenyltetrazolium chloride to visualize viable myocardium. For *in vivo* hemodynamic measurements, mice were anesthestized with pentobarbital (6 mg/100 g body weight i.p). Mice under anesthesia for longer than 30 minutes were given a second dose of pentobarbital (3mg/100mg body weight). A high fidelity solid state 1.2 PV catheter (Transonic Systems Inc.) was inserted into the left ventricle. Signal was optimized by phase and magnitude channels (Porterfield et al., 2009) and data was collected by PowerLab 8/36 and LabChart 7 Pro (ADInstruments). Dobutamine was infused in to the right jugular as described previously (Liu et al., 2009). Adult cardiac myocytes were isolated as previously described (Goonasekera et al., 2012). For the sprinting regimens, 18 week-old animals were acclimatized to the treadmill (Omni-Pacer LC4/M; Columbus Instruments International) for 5 minutes prior to shock grid activation and then given either a short 2-minute warm-up or a prolonged 30-minute warm-up, followed by 20 minutes of sprinting at 20 m/min. For the short 2-minute warm-up, the treadmill speed was set at 10 m/min for 1 minute and then increased to 15 m/min for 1 minute before beginning the 20-minute, 20 m/min sprint. For the prolonged 30-minute warm-up, animals were run for 5-minute increments starting at 10 m/min and increasing in speed by 1 m/min until a speed of 15 m/min was reached. After 5 minutes at 15 m/min, the 20 minute, 20 m/min sprint challenge was initiated. Running capacity was assessed as the maximum sprint time before exhaustion. Exhaustion was determined by the animal remaining on the mild shock grid for 10 consecutive seconds.

**Respiration in adult cardiomyocytes**

Respiration in adult cardiomyocytes was measured using a Seahorse XF24 Flux Analyzer (Seahorse Biosciences) as described in (Readnower et al., 2012). In brief, myocytes were plated on the XF24 cell culture microplates coated with laminin (40 μg/ml). Respiration was measured in XF Base Medium (Seahorse Biosciences) containing 1 mM pyruvate, 4 mM

glutamine, 5 mM glucose. β-adrenergic stimulation of cardiac myocytes was achieved with the addition of 3.25 nM isoproterenol. Five micromolar Ru360 was used as a control.

**Mitochondrial isolation and analyses**

Cardiac mitochondria were isolated as previously described (Kwong et al., 2014). Briefly, hearts were harvested, homogenized in MS-EGTA buffer (225 mM mannitol, 75 mM sucrose, 5 mM Hepes, and 1 mM EGTA, pH 7.4) and subjected to differential centrifugation. For mitochondrial $Ca^{2+}$ uptake, mitochondria were suspended in buffer containing125 mM KCl, 20 mM Hepes, 2 mM $MgCl_2$, 2 mM potassium phosphate, and 40 μM EGTA, pH 7.2, 500μM calcium green-5N (Molecular Probes), 7 mM pyruvate and 1 mM malate. Mitochondria were challenged with additions of 100 μM or 200 μM $CaCl_2$ and calcium green-5N fluorescence was monitored using the BioTek Synergy II plate reader (BioTek). As a control, mitochondria were pre-incubated with 1 μM Ru360 (EMD Millipore) prior to the start of the experiment. For mitochondrial $Ca^{2+}$ content, mitochondria were suspended in buffer containing 120 mM KCl, 5 mM $KH_2PO_4$, and 10 mM Tris pH 7.4, solubilized by freeze-thawing and sonication, and cleared by centrifugation. $Ca^{2+}$ content was measured using a Calcium Detection Kit (Abcam). Mitochondrial ATP synthesis rates were measured as described in (Vives-Bauza et al., 2007). Briefly, ATP synthesis was measured by suspending mitochondria in buffer containing 150 mM KCl, 25 mM Tris-HCl, 10 mM $K_2HPO_4$, 2 mM EGTA, 0.1 mM $MgCl_2$ and 0.1% fatty acid free BSA pH 7.4. 150 μM diadenosine pentaphosphate, 1 mM malate, 1 mM pyruvate, 100 μM ADP, 40 μM luciferin and 1 μg/ml luciferase were sequentially added. Luminescence was monitored over 3 minutes using a luminometer (BioTek Synergy II) and the rate of ATP synthesis was taken as the slope of linear increase in luminescence. $Ca^{2+}$ stimulation of ATP synthesis was achieved with the addition of 400 μM $CaCl_2$ and MCU inhibition was achieved with incubation with 5 μM Ru360. Oxygen consumption was measured using a Clarke type electrode (Hansatech) as described in (Pan et al., 2013). Respiration was measured in buffer containing 120 mM KCl, 5 mM MOPS, 0.1 mM EGTA, 5 mM $KH_2PO_4$, 0.2% BSA, 10 mM glutamate and 2 mM malate. State 3 respiration was initiated with the addition of 0.5 mM ADP, $Ca^{2+}$ stimulated respiration was achieved with the addition of 0.1 mM $CaCl_2$ and 5 μM Ru360 was added for MCU inhibition. Mitochondrial swelling assays were conducted as previously described (Kwong et al., 2014). Briefly, mitochondria were suspended in buffer containing 120 mM KCl, 10 mM Tris pH 7.4, 5 mM $KH_2PO_4$, 7 mM pyruvate, 1 mM malate, and 10 μM EDTA,

challenged with 200 μM $CaCl_2$, and absorbance at 540 nm was monitored. As controls, mitochondria were treated with either 5 μM cyclosporine A or 2 μM Ru360.

**Cardiomyocyte ROS production and biochemical assays.**

ROS production in adult cardiomyocytes was measured using a DCFDA Cellular ROS Detection Assay (Abcam). Cardiac NADPH levels were measured in heart lysate using the NADP/NADPH Assay Kit (Abcam). Cardiac catalase activity was measured in heart lysates using a Catalase Assay Kit (Abcam). Serum lactate levels were analyzed by the Cincinnati Children's Hospital Medical Center Clinical Diagnostics Lab.

**$Ca^{2+}$ and MPTP measurements in cardiomyocytes**

To measure mitochondrial $Ca^{2+}$, adult myocytes were pretreated with 5 μM thapsigargin, permeabilized and loaded with Rhod-2 and challenged with 2 μM $Ca^{2+}$. To quantify the extent of mitochondrial $Ca^{2+}$ uptake, Rhod2 was measured 14 min after addition of $Ca^{2+}$. To calibrate basal mitochondrial $Ca^{2+}$, the myocytes pretreated as above were equilibrated with internal solution of 100 nM [$Ca^{2+}$] (mimicking basal cytosolic [$Ca^{2+}$]). $F_{min}$ and $F_{max}$ were measured at 0 and 4 μM [$Ca^{2+}$] respectively, and the internal solution contained 5 μM ionomycin ($Ca^{2+}$ ionophore, 5 μM carbonyl cyanide-4 (trifluoromethoxy) phenylhydrazone and 1 μM oligomycin to dissipate mitochondrial membrane potential. To measure mitochondrial $Ca^{2+}$ efflux, myocytes were exposed to lower [ionophore] (1 μM), and mitochondria were loaded with Rhod-2 and 2 μM $CaCl_2$ (for equal $Ca^{2+}$ loading, control myocytes were treated with 2 μM Ru360). Mitochondrial $Ca^{2+}$ leak was measured as the decrease in Rhod-2 fluorescence upon switch to media devoid of both $Ca^{2+}$ and $Na^{+}$. Mitochondria were exposed to 2 μM $CaCl_2$ and then we measured the decline in Rhod-2 fluorescence following a switch to buffer containing no $Ca^{2+}$ and 10 mM $Na^{+}$. Here, mNCX mediated $Ca^{2+}$ efflux was assessed by normalizing the $Ca^{2+}$ decline rate in the presence of $Na^{+}$ to that in the absence of $Na^{+}$. MPTP opening in permeablized adult myocytes was measured with 10 nM TMRM in buffer containing 100 nM free $Ca^{2+}$ and 0.05 mM EGTA. The frequency of MPTP opening is the number of opening MPTP normalized by total number of mitochondrial in 10 min. Experiments were performed with confocal microscopy (Zeiss, LSM 5 Live, ×63 objective) using 2D frame mode with DPSS laser (excitation at 532 nm, emission at >560 nm). Image analysis used ImageJ software and LSM Image Examiner.

**$Ca^{2+}$ sparks and transients measurements**

Intact ventricular myocytes were loaded with Fluo-4 AM dye (5 µM Molecular Probes), transients and sparks were recorded as previously described (Erickson et al., 2013; van Oort et al., 2010). $Ca^{2+}$ transients were obtained by field stimulation at 1 Hz in normal Tyrode. SR $Ca^{2+}$ load was evaluated by the $Ca^{2+}$ transient upon rapid caffeine application (10 mM). Images were acquired with confocal microscopy (BioRad, Radiance 2100, ×40 objective) using line scan mode with argon 4 laser (excitation at 488 nm, emission at >505 nm). Image analysis used ImageJ software and $Ca^{2+}$ Sparkmaster.

**Statistics**

All results are presented as mean ± SEM. Statistical significance was determined by Student's t-test and $p<0.05$ were considered significant.

**References**


Erickson, J.R., Pereira, L., Wang, L., Han, G., Ferguson, A., Dao, K., Copeland, R.J., Despa, F., Hart, G.W., Ripplinger, C.M., et al. (2013). Diabetic hyperglycaemia activates CaMKII and arrhythmias by O-linked glycosylation. Nature *502*, 372-376.

Fewell, J.G., Osinska, H., Klevitsky, R., Ng, W., Sfyris, G., Bahrehmand, F., and Robbins, J. (1997). A treadmill exercise regimen for identifying cardiovascular phenotypes in transgenic mice. Am J Physiol *273*, H1595-1605.

Goonasekera, S.A., Hammer, K., Auger-Messier, M., Bodi, I., Chen, X., Zhang, H., Reiken, S., Elrod, J.W., Correll, R.N., York, A.J., et al. (2012). Decreased cardiac L-type Ca(2)(+) channel activity induces hypertrophy and heart failure in mice. J Clin Invest *122*, 280-290.

Kaiser, R.A., Bueno, O.F., Lips, D.J., Doevendans, P.A., Jones, F., Kimball, T.F., and Molkentin, J.D. (2004). Targeted inhibition of p38 mitogen-activated protein kinase antagonizes cardiac injury and cell death following ischemia-reperfusion in vivo. J Biol Chem *279*, 15524-15530.

Kwong, J.Q., Davis, J., Baines, C.P., Sargent, M.A., Karch, J., Wang, X., Huang, T., and Molkentin, J.D. (2014). Genetic deletion of the mitochondrial phosphate carrier desensitizes the mitochondrial permeability transition pore and causes cardiomyopathy. Cell Death Differ *21*, 1209-1217.

Liu, Q., Chen, X., Macdonnell, S.M., Kranias, E.G., Lorenz, J.N., Leitges, M., Houser, S.R., and Molkentin, J.D. (2009). Protein kinase C{alpha}, but not PKC{beta} or PKC{gamma}, regulates contractility and heart failure susceptibility: implications for ruboxistaurin as a novel therapeutic approach. Circ Res *105*, 194-200.

Nakayama, H., Bodi, I., Correll, R.N., Chen, X., Lorenz, J., Houser, S.R., Robbins, J., Schwartz, A., and Molkentin, J.D. (2009). alpha1G-dependent T-type Ca2+ current antagonizes cardiac hypertrophy through a NOS3-dependent mechanism in mice. J Clin Invest *119*, 3787-3796.

Pan, X., Liu, J., Nguyen, T., Liu, C., Sun, J., Teng, Y., Fergusson, M.M., Rovira, II, Allen, M., Springer, D.A., et al. (2013). The physiological role of mitochondrial calcium revealed by mice lacking the mitochondrial calcium uniporter. Nat Cell Biol *15*, 1464-1472.

Porterfield, J.E., Kottam, A.T., Raghavan, K., Escobedo, D., Jenkins, J.T., Larson, E.R., Trevino, R.J., Valvano, J.W., Pearce, J.A., and Feldman, M.D. (2009). Dynamic correction for parallel conductance, GP, and gain factor, alpha, in invasive murine left ventricular volume measurements. J Appl Physiol (1985) *107*, 1693-1703.

Readnower, R.D., Brainard, R.E., Hill, B.G., and Jones, S.P. (2012). Standardized bioenergetic profiling of adult mouse cardiomyocytes. Physiol Genomics *44*, 1208-1213.

Sohal, D.S., Nghiem, M., Crackower, M.A., Witt, S.A., Kimball, T.R., Tymitz, K.M., Penninger, J.M., and Molkentin, J.D. (2001). Temporally regulated and tissue-specific gene manipulations in the adult and embryonic heart using a tamoxifen-inducible Cre protein. Circ Res *89*, 20-25.

van Oort, R.J., Respress, J.L., Li, N., Reynolds, C., De Almeida, A.C., Skapura, D.G., De Windt, L.J., and Wehrens, X.H. (2010). Accelerated development of pressure overload-induced cardiac hypertrophy and dysfunction in an RyR2-R176Q knockin mouse model. Hypertension *55*, 932-938.

Vives-Bauza, C., Yang, L., and Manfredi, G. (2007). Assay of mitochondrial ATP synthesis in animal cells and tissues. Methods Cell Biol *80*, 155-171.

Wilkins, B.J., Dai, Y.S., Bueno, O.F., Parsons, S.A., Xu, J., Plank, D.M., Jones, F., Kimball, T.R., and Molkentin, J.D. (2004). Calcineurin/NFAT coupling participates in pathological, but not physiological, cardiac hypertrophy. Circ Res *94*, 110-118.

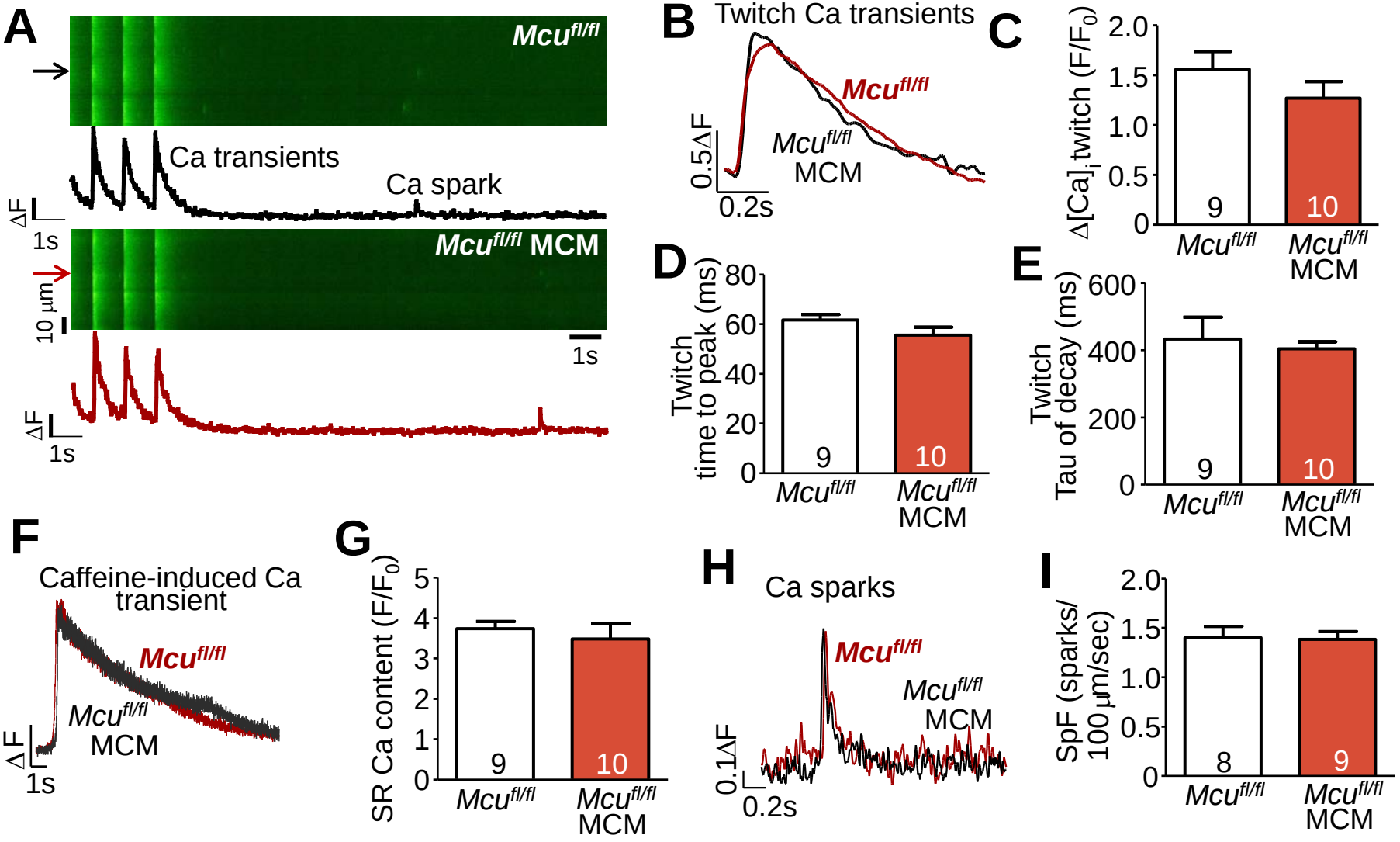


**Figure S1.** Assessment of $[Ca]_i$ in control and *Mcu*-deleted adult mouse cardiomyocytes (Relates to Figure 1). Line scans images (A) show three twitch Ca transients and some Ca sparks (line plots below are for the locations indicated by the arrows). Data show that loss of *Mcu* has no effect on intracellular Ca handling, not in twitch Ca transient magnitude (B,C), time to peak or decay (B,D and E), or sarcoplasmic reticulum (SR) Ca load assessed by caffeine-induced Ca transients (F,G) or in Ca spark frequency under paced conditions (H,I). Myocytes were loaded with Fluo-4 for $[Ca]_i$ detection.

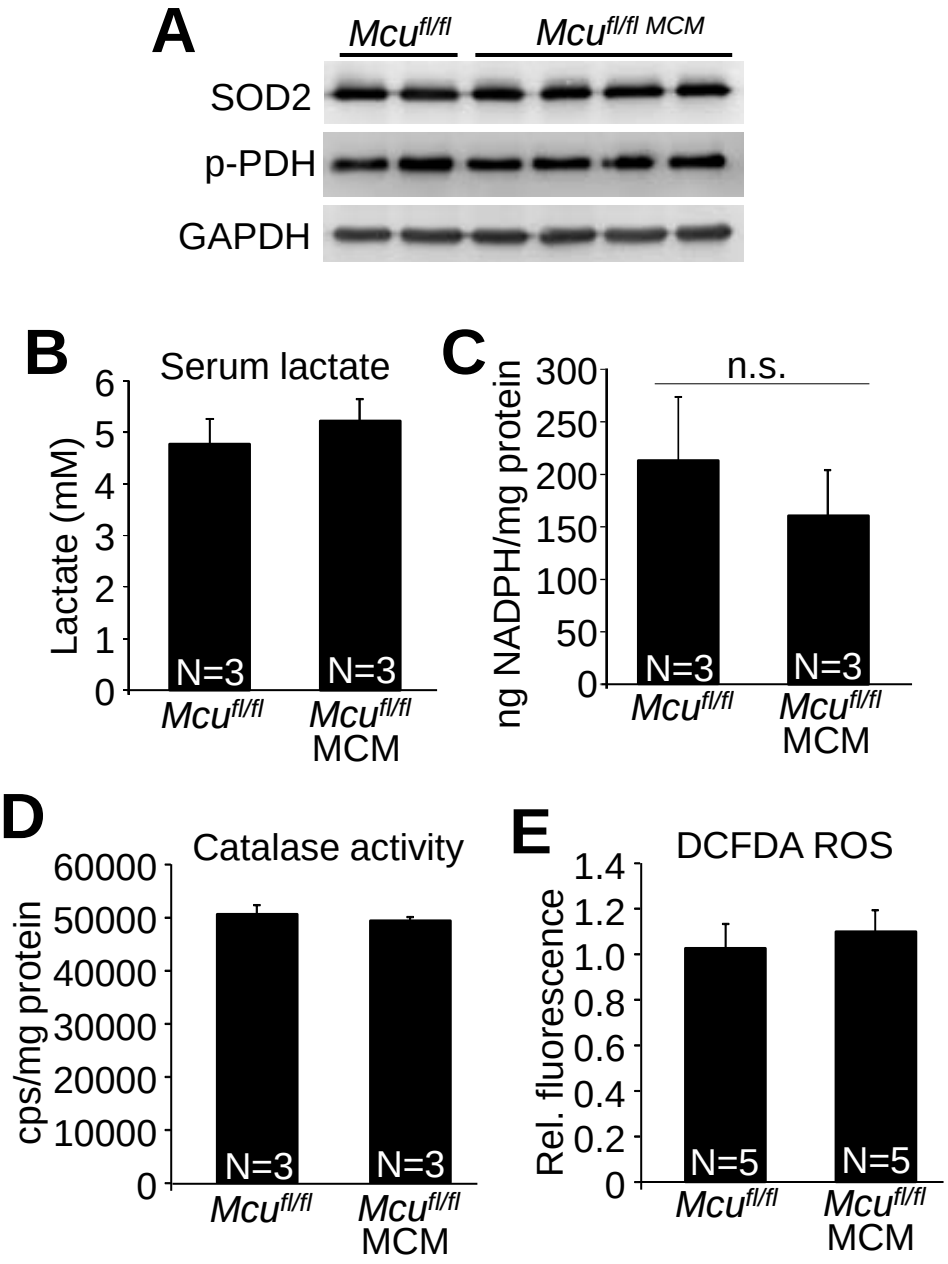


**Figure S2**. Assessment of other potential metabolic or compensatory derangements due to cardiac *Mcu* deletion (Relates to Figure 4). (A) Western blot analysis of SOD2 expression and PDH1Ea serine 293 phosphorylation in total heart lysates prepared from the indicated mice. GAPDH was used as a protein loading control. (B) Quantification of serum lactate levels in the indicated groups. Assessment of NADPH content (C) and catalase activity (D) in heart homogenates prepared from the indicated groups. (E) ROS production in adult cardiomyocytes isolated from the indicated groups as measured by DCFDA fluorescence.

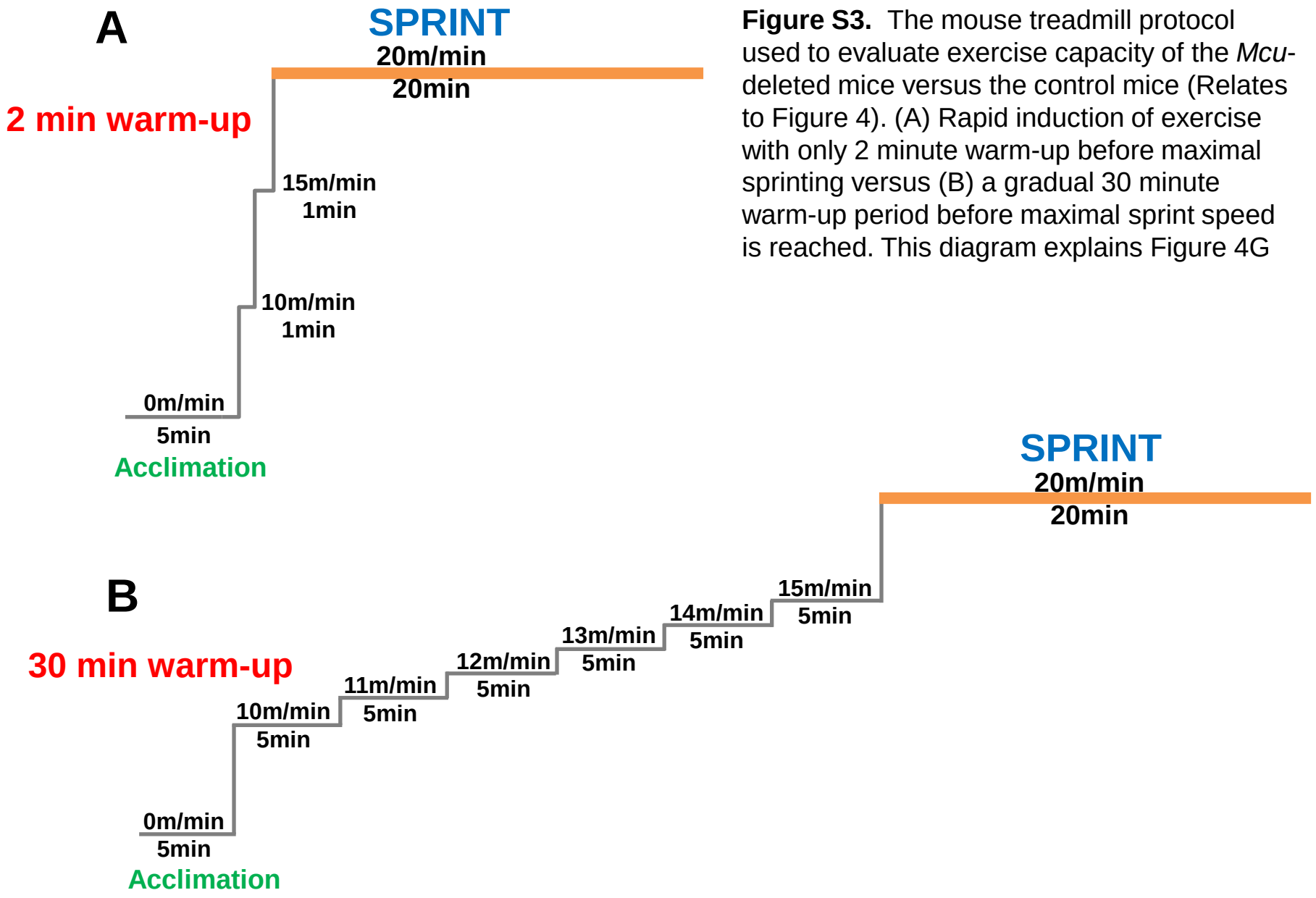


**Figure S3.** The mouse treadmill protocol used to evaluate exercise capacity of the *Mcu*-deleted mice versus the control mice (Relates to Figure 4). (A) Rapid induction of exercise with only 2 minute warm-up before maximal sprinting versus (B) a gradual 30 minute warm-up period before maximal sprint speed is reached. This diagram explains Figure 4G

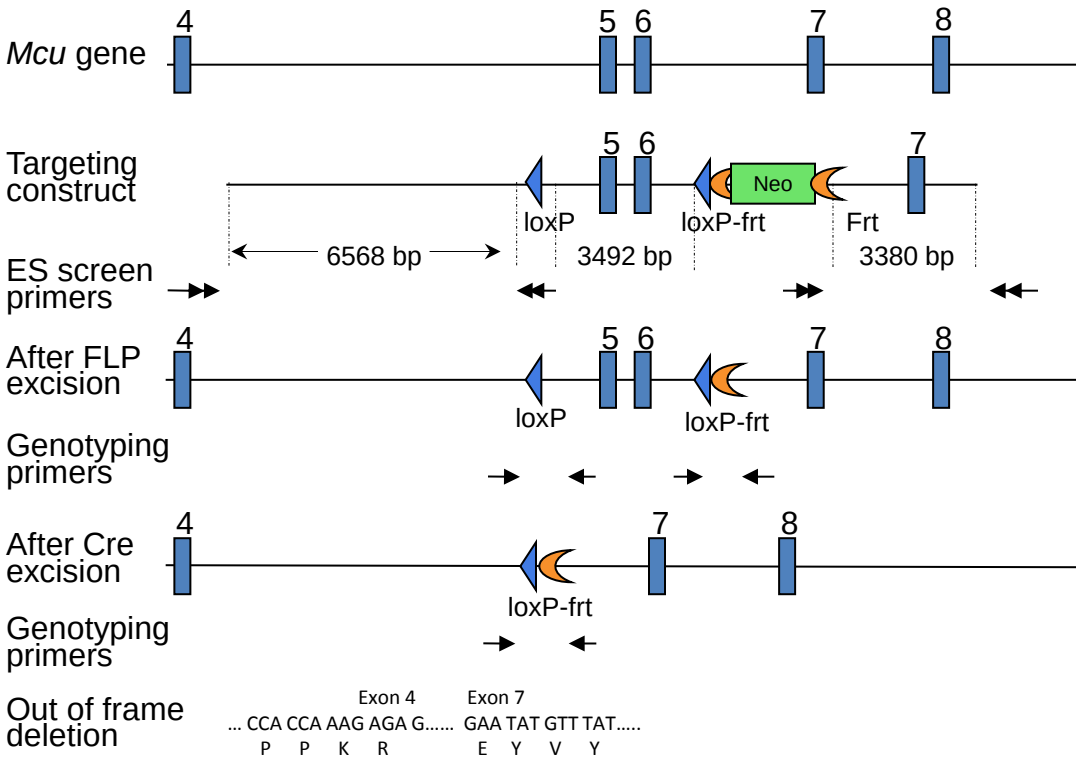


**Figure S4**. Schematic of the *Mcu* gene targeting strategy in ES cells that was used to make gene-targeted mice for inducible deletion of this gene (linked to Experimental Procedures). LoxP sites are shown as blue triangle and the FRT sites are the half circles in orange. The exons of the *Mcu* gene are numbers as blue rectangle and the arrows show the position of the various PCR primers that were used. The steps of the actual targeting in ES cells are described in the Extended Methods section.